KLP-6 is a kinesin superfamily protein resistant to ADP inhibition

Tomoki Kita[1,#] and Shinsuke Niwa[1,2,#]

1 Graduate School of Life Sciences, Tohoku University, Miyagi 980-8577, Japan.

2 Frontier Research Institute for Interdisciplinary Sciences (FRIS), Tohoku University, Miyagi 980-0845, Japan.

Corresponding author: TOMOKI KITA, Graduate School of Life Sciences, Tohoku University, Katahira 2-1-1, Aoba-Ku, Sendai, Miyagi 980-8577, Japan.

e-mail: tomoki.kita.p3@dc.tohoku.ac.jp

Corresponding author: SHINSUKE NIWA, Frontier Research Institute for Interdisciplinary Sciences (FRIS), Tohoku University, Aramaki-Aoba 6-3, Aoba-Ku, Sendai, Miyagi 980-0845, Japan.

e-mail: shinsuke.niwa.c8@tohoku.ac.jp

Abstract

Product inhibition is a type of enzyme inhibition in which the reaction product suppresses further enzyme activity. Kinesins are microtubule-dependent ATPases that move along microtubules by hydrolyzing ATP into ADP and inorganic phosphate (Pi). Like other ATPases, kinesins are inhibited by their hydrolysis product, ADP. In this study, we identified that the *Caenorhabditis elegans* kinesin-3, KLP-6, is minimally affected by ADP inhibition and continues to move along microtubules at an unreduced speed even in the presence of high concentration of ADP. The Michaelis constants for Mg·ATP (K_{M}) and the inhibition constant for Mg·ADP (K_{I}) were measured, revealing that the $K_{\mathrm{I}}/K_{\mathrm{M}}$ ratio of 44.9 for KLP-6 is significantly higher than the ratio of 1.3 observed for the well-studied kinesin-3, KIF1A. This indicates that KLP-6 exhibits a much higher preference for ATP over ADP. Amino acid sequence and structural comparisons between KLP-6 and other kinesin-3 members revealed that KLP-6 possesses a unique α2a helix and loop-5. Substituting these regions with those from KIF1A abolished KLP-6's higher selectivity for ATP over ADP, confirming that these domains are crucial for its minimal ADP inhibition. Studying KLP-6 provides valuable insights into kinesin's substrate selectivity and associated motor functions.

Introduction

Product inhibition is a common phenomenon in enzyme-catalyzed reactions (1). Since most product molecules of an enzyme reaction share structural similarities with the substrate, they can still bind to the enzyme's active site, preventing substrate binding and reducing the reaction velocity. Product inhibition plays a crucial role in regulating cellular metabolism, serving as a negative feedback mechanism to control metabolic pathways (2). Overcoming this inhibition is also important in the biotechnology industry to enhance product yield (3–5).

Some enzymes have been reported to be resistant to product inhibition. Glucokinase, also known as hexokinase IV or D, is one of the four members of the hexokinase enzyme family. It phosphorylates glucose, using ATP as the second substrate, to form glucose-6-phosphate. Unlike other hexokinases, glucokinase has a lower affinity for glucose and is insensitive to physiological concentrations of glucose-6-phosphate (6). As a result, the activity of this enzyme is primarily regulated by glucose concentration alone (6). β-glucosidases hydrolyze cellooligosaccharides, such as cellobiose and cellotriose, into D-glucose. Td2F2 and MeBglD2, members of the glycoside hydrolase family 1, are not inhibited and, surprisingly, are activated in the presence of D-glucose (7, 8). Due to their minimal product inhibition, they are considered promising candidates for enhancing biomass saccharification (8).

Most molecular motor proteins hydrolyze ATP, generating ADP and Pi, to move or rotate directionally. Myosins are well known for their roles in muscle contraction, and their activity on actin filaments is influenced by ADP product inhibition (9, 10). Notably, skeletal muscle myosin is less affected by ADP inhibition compared to cardiac and smooth muscle myosins, highlighting differences in how ADP modulates contractile function across muscle types (11, 12). F1-ATPase is a rotary molecular motor in which the central γ-subunit rotates against the α3β3 cylinder. When Mg·ADP is produced during ATP hydrolysis or binds from the external medium, the motor enters an

inhibited state and rarely releases the bound Mg·ADP (13–15). A mutation in the nucleotide-binding site, known as the Walker A motif or P-loop, has been shown to reduce ADP inhibition in F1-ATPase, enabling detailed studies of its energetics (16, 17). In eukaryotic cilia and flagella, axonemal dyneins coordinate their functions to generate oscillatory bending of axonemes. Axonemal dynein contains four nucleotide-binding sites (18, 19). Interestingly, its activity is enhanced in the presence of ADP in addition to ATP (20, 21), suggesting that additional ADP binding plays a physiological role in regulating dynein activity (22). Kinesins are primarily responsible for intracellular transport and move along microtubules. The movement of kinesin-1, also called conventional kinesin, is strongly inhibited by ADP but not by Pi (23). Although kinesin proteins are classified into 15 families (24), no species exhibiting minimal ADP inhibition or mutations conferring this functionality have been reported.

Here, we report that the *Caenorhabditis elegans* (*C. elegans*) kinesin-3, KLP-6, is minimally affected by ADP inhibition and exhibits a high selectivity for ATP over ADP. KLP-6 is responsible for transporting a mechanosensory receptor complex in male-specific *ce*phalic *m*ale (CEM) cilia (25, 26). KLP-6 moved along microtubules at an unchanged speed in the presence of equal concentrations of ADP and ATP, in contrast to another kinesin-3 member, KIF1A, which exhibited a significantly reduced speed in the presence of ADP. Through amino acid sequence and structural comparisons between KLP-6 and other kinesin-3 members, we experimentally identified that the specific α2a helix and loop-5 play a key role in its minimal ADP inhibition.

Results

KLP-6 exhibits directional movement along microtubules in an ADP solution.

We compared the single-molecule activities of two kinesin-3 proteins, human KIF1A and *C. elegans* KLP-6, using total internal reflection fluorescence (TIRF) microscopy. To directly

investigate the motility parameters of these motors, we analyzed truncated versions containing the motor and neck coiled-coil domains (Fig. 1A). Since the neck coiled-coil domains of KIF1A and KLP-6 do not form stable dimers (27–29), the motors were stably dimerized via fusion to a leucine zipper (KIF1A(1-393)LZ and KLP-6(1-390)LZ) (28, 30–34) (Fig. 1A).

Normally, kinesins lack processivity along microtubules in ADP solution (35). A well-studied KIF1A(1-393)LZ did not exhibit unidirectional movement in the presence of 2 mM Mg·ADP purchased from Nacalai Tesque (33, 34, 36) (Fig. 1B). Surprisingly, we observed that KLP-6(1-390)LZ moved along microtubules at a speed of 55±2 nm/s (mean±S.E.) in the same condition (Figs. 1B and C). Although the speed was much slower than in the presence of 2 mM Mg·ATP (260 nm/s) (28), KLP-6 obviously possessed processivity even in ADP solutions. One possible explanation for this movement is that KLP-6(1-390)LZ hydrolyzes ATP that was originally present as a contaminant in the purchased ADP stock (37, 38). To test this hypothesis, we depleted ATP from the ADP stock using hexokinase (38, 39) and observed the motility of KLP-6(1-390)LZ in a hexokinase-treated ADP (HK-ADP) solution. As a result, KLP-6(1-390)LZ lost its processivity (Fig. 1D), suggesting that KLP-6 can bind trace amounts of ATP even in the presence of excess ADP.

KLP-6 is minimally affected by ADP inhibition.

To quantify ADP inhibition in KLP-6, we measured motor velocity on microtubules at various Mg·ATP concentrations ([Mg·ATP]) in the presence or absence of 1 mM Mg·HK-ADP. Under all conditions used in this study, the dependence of the single-molecule velocity on [Mg·ATP] was well described by the standard Michaelis–Menten equation (23):

$$V = \frac{V_{\mathrm{max}}\,[\mathrm{Mg}\cdot\mathrm{ATP}]}{K_{\mathrm{M}} + [\mathrm{Mg}\cdot\mathrm{ATP}]}$$

where V_{max} represents the maximum speed, and K_{M} denotes the [Mg·ATP] concentration required to achieve half-maximal velocity. In the presence of Mg·HK-ADP, V is described as

$$V = \frac{V_{\max}\,[\mathrm{Mg}\cdot\mathrm{ATP}]}{K_{\mathrm{M}}(1+[\mathrm{Mg}\cdot\mathrm{HK}-\mathrm{ADP}]/K_{\mathrm{I}})+[\mathrm{Mg}\cdot\mathrm{ATP}]}$$

where K_{I} represents the inhibition constant for Mg·HK-ADP.

First, we analyzed KIF1A(1-393)LZ as a control. In the presence of equimolar ADP and ATP, the motor velocity was significantly reduced compared to that observed in the ATP-only solution (Figs. 2A and B), consistent with previous observations for the conventional kinesin (23). In contrast, the velocity of KLP-6(1-393)LZ remained unchanged, even in the presence of equal concentrations of ADP and ATP (Figs. 2C and D). From these plotting, we determined the kinetic parameters for KIF1A(1-393)LZ: $V_{\max}$ = 2381±23 nm/s (mean±S.E.), K_{M} = 190±3 μM (mean±S.E.), and K_{I} = 247±3 μM (mean±S.E.) (Figs. 2E-G and Table. 1). $V_{\max}$ and K_{M} are in agreement with prior studies (30–32, 40). For KLP-6(1-390)LZ, the corresponding parameters were $V_{\max}$ = 248±3 nm/s (mean±S.E.) and K_{M} = 20.1±0.5 μM (mean±S.E.) which are comparable to those of *C. elegans* kinesin-2 (41) and conventional kinesin (23), respectively (Figs. 2E, F and Table. 1). In contrast, the K_{I} of KLP-6(1-390)LZ was 901±31 μM (mean±S.E.) (Fig. 2G), the highest value reported among the kinesin superfamily proteins measured to date.

To quantify the selectivity for ATP over ADP, we defined the selectivity ratio as $K_{\mathrm{I}}/K_{\mathrm{M}}$. Although this ratio does not directly correspond to the binding constant ratio of the ADP and ATP ($K_{\mathrm{ADP}}/K_{\mathrm{ATP}}$), it serves as a useful proxy (11). The selectivity ratio for KIF1A was 1.3±0.1 (mean±S.E.), which is comparable to that of conventional kinesin (23) (Fig. 2H and Table. 1). This indicates that KIF1A is significantly affected by ADP inhibition and exhibit no strong preference between ATP and ADP binding. In contrast, due to the high K_{I} value of KLP-6(1-390)LZ, the selectivity ratio of KLP-6(1-390)LZ was 44.9±1.9 (mean±S.E.), which is much higher than that of KIF1A(1-393)LZ (Fig. 2H and Tabel. 1). These findings highlight that KLP-6 is a unique kinesin that exhibits remarkable resistance to ADP inhibition.

Unique amino acid sequence of KLP-6

To identify the regions responsible for minimum ADP inhibition in KLP-6, we compared its amino acid sequence with those of other kinesin-3s from humans and *C. elegans* (Fig. 3A). A notable distinction of KLP-6 compared to other kinesin-3s is a unique insertion in loop-3. Unlike the loop-3 of KIF1A, the longer loop-3 of KLP-6 extends over the nucleotide-binding site (42, 43) (Figs. 3B and C). Kinesin-3 family proteins naturally possess an extended loop-3 (44), and the additional extension of this loop in KLP-6 may contribute to its significantly higher preference for ATP over ADP.

The P-loop contains the consensus sequence GX_4GK(T/S). In F1-ATPase, replacing the C-terminal threonine in the P-loop of the β subunit with serine has been shown to reduce ADP inhibition (16, 17). In kinesin-3 family members, the P-loop naturally terminates with serine; however, differences in the adjacent α2a helix distinguish KLP-6 from other kinesin-3 proteins (Fig. 3A). In most kinesin-3s, the conserved sequence at the end of the α2a helix is TMM, whereas KLP-6 uniquely features the sequence SIV (Fig. 3A). The first threonine and second methionine are also conserved in kinesin-1 and kinesin-2 family members (Fig. S1), suggesting that this sequence plays a crucial role in nucleotide binding and/or ATP hydrolysis.

From a structural perspective, the number of hydrogen bonds between ADP and KLP-6 is fewer than that in KIF1A (Figs. S2A and B). Notably, while loop-5 of KIF1A contains a lysine that forms a hydrogen bond with ADP-ribose, the corresponding position in KLP-6 is occupied by phenylalanine, which lacks this interaction (Figs. 3B and C). This destabilization of nucleotide binding may contribute to KLP-6's high resistance to ADP inhibition.

Loop-5 and α2a helix of KLP-6 contribute to minimum ADP inhibition in KLP-6

Based on sequence comparisons between KLP-6 and other kinesin-3 proteins, we

generated three mutant KLP-6 constructs (Figs. 4A and B) and analyzed the impact of ADP inhibition on their activity (Figs. 4C-F). First, we tested whether the long loop-3 is responsible for the KLP-6’s high selectivity for ATP over ADP. A ‘swap’ construct, KLP-6(1-390)LZ(L3SW), was created by replacing the native loop-3 of KLP-6 with the loop-3 from KIF1A (Figs. 4A and B). While the velocity in the presence of 1 mM Mg·ATP was unaffected by the addition of 1 mM HK-Mg·ADP, similar to the wild type (Figs. 4C and D), the loop-3 swap caused a slight decrease in V_{max} to 203±5 nm/s (mean±S.E.) and increases in both K_{M} and K_{I}, measured at 31.3±1.7 μM and 1175±78 μM (mean±S.E.), respectively (Figs. 4G-I and Table. 1). Consequently, the selectivity ratio ($K_{\mathrm{I}}/K_{\mathrm{M}}$) was reduced to 37.5±2.9 (mean±S.E.), a slight decrease compared to the wild type (Fig. 4J and Table. 1). These results suggest that the extended loop-3 affects the nucleotide-binding site and modulates nucleotide affinity. However, since KLP-6(1-390)LZ(L3SW) still exhibited significantly higher preference for ATP over ADP (Fig. 4J), loop-3 is not the primary determinant of KLP-6’s minimal ADP inhibiton.

Next, we introduced the F120K mutation into KLP-6(1-390)LZ (Figs. 4A and B), which was expected to create a hydrogen bond with ADP (Fig. 3B). Interestingly, F120K turned out to be a gain-of-function mutation, increasing V_{max} to 338±4 nm/s (mean±S.E.) (Figs. 4C, E, G, and Table. 1). In the presence of equimolar ADP and ATP, KLP-6(1-390)LZ(F120K) was not inhibited by ADP, consistent with the wild type (Figs. 4C and E). However, when ADP was present at a 10-fold higher concentration than ATP, the reduction in motor velocity was more pronounced compared to the wild type (Figs. 4C and E). Further analysis revealed that while its K_{M} of 20.3±0.5 μM (mean±S.E.) was comparable to that of the wild type (Fig. 4H and Tbale. 1), its K_{I} was significantly reduced to 242±4 μM (mean±S.E.), resulting in decreased selectivity for ATP over ADP ($K_{\mathrm{I}}/K_{\mathrm{M}}$ = 11.9±0.6, mean±S.E.) (Figs. 4I, J, and Table. 1). These findings indicate that the loop-5 of KLP-6 is designed to avoid forming a hydrogen bond with ADP, contributing to its resistance to ADP inhibition.

Finally, we investigated the role of KLP-6's specific α2a helix in ADP inhibition. Three mutations—S116T, I117M, and V118M—were introduced into KLP-6(1-390)LZ, generating the construct KLP-6(1-390)LZ(SIV/TMM) (Figs. 4A and B). In the presence of equimolar ADP and ATP, we observed that KLP-6(1-390)LZ(SIV/TMM) was inhibited by ADP, similar to KIF1A (Figs. 4C and F). Notably, the K_{M} decreased approximately fivefold to 4.4±0.1 μM (mean±S.E.), and the K_{I} was significantly reduced by a factor of 76 to 11.9±0.3 μM (mean±S.E.), while the $V_{\max}$ remained largely unchanged at 234±3 nm/s (mean±S.E.) (Figs. 4G-I and Table. 1). The $K_{\mathrm{I}}/K_{\mathrm{M}}$ ratio was calculated to be 2.7±0.3 (mean±S.E.), almost consistent with KIF1A and conventional kinesin (Fig. 4J and Table. 1). These results demonstrate that the SIV/TMM mutations increased the affinity for both ATP and ADP, thereby abolishing the high specificity for ATP. We conclude that the α2a helix of KLP-6 is a key determinant of its higher preference for ATP over ADP.

Discussion

In this study, we find that KLP-6 is resistant to ADP inhibition and determine the regions responsible for this unique characteristic. We successfully identified that the α2a helix of KLP-6 plays the most significant role in its minimal ADP inhibition (Fig. 4J). Substituting the sequence of the α2a helix (SIV motif) with that of another kinesin-3 (TMM motif) significantly increased the affinity for both ATP and ADP, indicating that the α2a helix of KLP-6 is naturally designed to reduce nucleotide affinity. Notably, glucokinase, which is resistant to product inhibition, is also characterized by low substrate affinity (6), suggesting that reduced substrate affinity may be a critical factor for achieving high substrate selectivity. Computational analysis revealed that the S116T, I117M, and V118M mutations do not significantly increase ADP affinity, but they enhance interactions with the β8 sheet, β7 sheet, and α3 helix, respectively (Fig. S3; see Supporting Information, Section 1 for more details). This suggests that the P-loop and α2a helix are less

stabilized in KLP-6 compared to other kinesin-3 family members, resulting in reduced nucleotide affinity and increased ATP selectivity.

Additionally, we find the contribution of loop-5. While KIF1A forms a hydrogen bond between loop-5 and ADP, KLP-6 lacks this interaction (Figure 3). Consistent with these structural comparison, the KLP-6(F120K) mutation increased affinity for ADP (Fig. 4I). However, the affinity for ATP was not significantly changed (Fig. 4H). Since ATP contains an additional phosphate group (γ-Pi), which is stabilized by hydrogen bonds with switch I and switch II in kinesins (45), the effect of an additional hydrogen bond on ATP affinity is likely limited. Interestingly, this mutation in loop-5 increased motor velocity by a factor of 1.3 (Fig. 4G). The mitotic kinesin Eg5 has a longer loop-5 compared to other kinesins, and this loop modulates conformational changes in key elements of the nucleotide-binding site by interacting with α3, which regulates speed and force generation in Eg5 (46). On the other hand, the role of loop-5 in other kinesins remains unclear. As the loop-5 of KLP-6 is not long enough to interact with α3 (Fig. S2D), it may instead directly facilitate ATP hydrolysis within the nucleotide-binding site in KLP-6(1-390)LZ(F120K).

In contrast to the SIV motif and loop-5, the contribution of loop-3 to KLP-6's high selectivity for ATP over ADP appears to be limited (Fig. 4J), although the hydrogen bonds between extended loop-3 and loop-5 is a distinctive feature of KLP-6 (Figs. S2C and D). Further analyses, such as molecular dynamics simulations, are needed to clarify the precise role of loop-3.

Since the ATP/ADP ratio in cells is typically around 10 (47), most kinesin motors are expected to be largely unaffected by ADP inhibition in vivo. However, the ATP/ADP ratio in CEM cilia remains unknown, and the significance of minimal ADP inhibition in KLP-6 is unclear. Unlike KLP-6, *C. elegans* kinesin-2, a ciliary kinesin, is highly susceptible to ADP inhibition (41) (Table. 1), suggesting that minimal ADP inhibition is not a common feature among ciliary kinesins. KLP-6 functions as a regulator of OSM-3 kinesin’s velocity and transport (26); thus, maintaining a stable

transport velocity, even in the presence of local ADP accumulation in the nonequilibrium cellular environment, may be crucial for efficient transport in CEM cilia.

Finally, we believe that studying KLP-6 will provide deeper insights into kinesin's substrate preference and related motor functions. Further structural analyses of KLP-6, such as its ATP-bound and microtubule-bound complexes, are expected to uncover the mechanisms underlying its high preference for ATP over ADP. KLP-6 could serve as a valuable model for developing molecular motors resistant to product inhibition, which may advance studies on motor's energetics (17) and contribute to the development of efficient molecular motor-based robots and systems (48, 49).

Methods

Expression of KLP-6 proteins

Reagents were purchased from Nacarai tesque (Kyoto, Japan), unless described. Expression of KLP-6 proteins was performed as described (28). The mutants were generated through PCR-based mutagenesis using KOD plus neo DNA polymerase (TOYOBO, Tokyo, Japan). To express KLP-6 (1–390)::LZ::mScarlet-I::Strep-tag II and its mutants, LOBSTR(DE3) was transformed and selected on an LB agar plate supplemented with kanamycin at 37°C overnight. Colonies were picked and cultured in 10 mL LB medium supplemented with kanamycin overnight. Next morning, 5 mL of the medium was transferred to 500 mL 2.5×YT (20 g/L tryptone, 12.5 g/L yeast extract, 6.5 g/L NaCl) supplemented with 10 mM phosphate buffer (pH 7.4) and 50 μg/mL kanamycin in a 2 L flask and shaken at 37°C. When OD600 reached 0.6, flasks were cooled in ice-cold water for 30 min. Then, 23.8 mg IPTG was added to each flask. Final concentration of IPTG was 0.2 mM. Flasks were shaken at 18°C overnight. Next day, bacteria expressing recombinant proteins were pelleted by centrifugation (3000×g, 10 min, 4°C), resuspended in PBS

and centrifuged again (3000×g, 10 min, 4°C). Pellets were resuspended in protein buffer (50 mM HEPES-KOH, pH 8.0, 150 mM KCH3COO, 2 mM MgSO4, 1 mM EGTA, 10% glycerol) supplemented with phenylmethylsulfonyl fluoride (PMSF).

Purification of KLP-6 proteins

Purification of KLP-6 proteins was performed as described (28). Bacteria were lysed using a French Press G-M (Glen Mills, NJ, USA) as described by the manufacturer. After being incubated with 1% streptomycin sulfate on ice for 20 min to eliminate nucleic acids from protein samples, lysates were cleared by centrifugation (75,000×g, 20 min, 4°C) and subjected to affinity chromatography described below. Lysate was loaded on Streptactin-XT resin (IBA Lifesciences, Göttingen, Germany) (bead volume: 2 mL). The resin was washed with 40 mL Strep wash buffer (50 mM HEPES-KOH, pH 8.0, 450 mM KCH3COO, 2 mM MgSO4, 1 mM EGTA, 10% glycerol). Protein was eluted with 40 mL Strep elution buffer (50 mM HEPES-KOH, pH 8.0, 150 mM KCH3COO, 2 mM MgSO4, 1 mM EGTA, 10% glycerol, 300 mM biotin). Eluted solution was concentrated using an Amicon Ultra 15 (Merck, Darmstadt, Germany) and then separated on an NGC chromatography system (Bio-Rad, Hercules, CA, USA) equipped with a Superdex 200 Increase 10/300 GL column (Cytiva, Tokyo, Japan). Peak fractions were collected and concentrated using an Amicon Ultra 4 (Merck). Proteins were analyzed by SDS-PAGE. Concentrated proteins were aliquoted and snap-frozen in liquid nitrogen.

Preparation of microtubules

Tubulin was purified from porcine brain as described (50). Tubulin was labeled with Biotin-PEG$_2$-NHS ester (Tokyo Chemical Industry, Tokyo, Japan) and AZDye647 NHS ester (Fluoroprobes, Scottsdale, AZ, USA) as described (51). To polymerize Taxol-stabilized microtubules

labeled with biotin and AZDye647, 30 μM unlabeled tubulin, 1.5 μM biotin-labeled tubulin and 1.5 μM AZDye647-labeled tubulin were mixed in BRB80 buffer (80 mM PIPES, 1mM $MgCl_2$, and 1mM EGTA) supplemented with 1 mM GTP and incubated for 15 min at 37°C. Then, an equal amount of BRB80 supplemented with 40 μM taxol was added and further incubated for more than 15 min. The solution was loaded on BRB80 supplemented with 300 mM sucrose and 20 μM taxol and ultracentrifuged at 100,000 g for 5 min at 30°C. The pellet was resuspended in BRB80 supplemented with 20 μM taxol.

ADP treatment with hexokinase

The ADP solution was treated with hexokinase (Sigma-Aldrich, St. Louis, MO, USA) and D-glucose to remove contaminating ATP as described (39). A 50 mM ADP solution was incubated with 200 mM D-glucose, 2 mM MgCl□, and 0.04 U/μl hexokinase at room temperature for 2 hours. After incubation, the enzyme was removed from the solution using an Amicon Ultra 0.5 filter (Merck). The solution was then aliquoted and stored at -20°C.

TIRF single-molecule motility assays

TIRF assays using porcine microtubules were performed as described (51). Glass chambers were prepared by acid washing as previously described (51). Glass chambers were coated with PLL-PEG-biotin (SuSoS, Dübendorf, Switzerland) and streptavidin (Wako). Polymerized microtubules were flowed into flow chambers and allowed to adhere for 5–10 min. Unbound microtubules were washed away using assay buffer (90 mM HEPES-KOH pH 7.4, 50 mM KCH_3COO, 2 mM $Mg(CH_3COO)_2$, 1 mM EGTA, 10% glycerol, 0.1 mg/ml biotin–BSA, 0.2 mg/ml kappa-casein, 0.5% Pluronic F127, specified nucleotides with Mg diluted to indicated concentrations, and an oxygen scavenging system composed of PCA/PCD/Trolox). Purified KIF1A and KLP-6 were

diluted to final concentrations of 10–20 pM and 100–400 pM, respectively, in the assay buffer. Then, the solution was flowed into the glass chamber. An ECLIPSE Ti2-E microscope equipped with a CFI Apochromat TIRF 100XC Oil objective lens (1.49 NA), an Andor iXion life 897 camera and a Ti2-LAPP illumination system (Nikon, Tokyo, Japan) was used to observe the motility. NIS-Elements AR software ver. 5.2 (Nikon) was used to control the system. All observations were completed before the motor slowed down due to ATP reduction.

Data analysis and graph preparation

All analyses were conducted using kymographs generated by ImageJ software (52). Unidirectional lines greater than 3 pixels along x axis (corresponding to approximately 318 nm) were counted as processive runs and the other signals were not counted. To quantify the maximum ATPase activity, segmented velocity was measured, with pause periods excluded. Nonlinear least-squares curve fitting was performed in python 3.0. Amino acid sequences of kinesins are aligned using CLUSTALW on ESPript 3 (53). Structural images were generated using PyMOL (Version 2.5, Schrödinger, LLC) and exported in PNG format. Hydrogen bonds between residues were also visualized using PyMOL. Graphs were created with python 3.0, exported in PNG format, and aligned using Adobe Illustrator 2023.

Supporting information

This article contains supporting information (54–56).

Acknowledgments

We would like to thank the members of Niwa lab for useful discussions. T.K. was supported by JSPS KAKENHI (grant no. JP23KJ0168). SN was supported by JSPS KAKENHI (grant no. JP23H02472).

Author contributions

T.K. writing–original draft; S.N. writing–review & editing; T.K. visualization; T.K. investigation; S.N. conceptualization; S.N. supervision; T.K. and S.N. funding acquisition.

Conflict of interest

The authors declare no competing interests.

Statement

During the preparation of this work the authors used ChatGPT4o in order to check English grammar and improve English writing. After using this tool, the authors reviewed and edited the content as needed and take full responsibility for the content of the publication.

References

1. **Holdgate, G. A., Meek, T. D., and Grimley, R. L. (2018) Mechanistic enzymology in drug discovery: a fresh perspective. *Nat Rev Drug Discov*. 17, 115–132**
2. **Sen, A. K., and Schulz, A. R. (1989) Effects of product inhibition in metabolic pathways: stability and control. *Math. Biosci.* 96, 255–277**
3. **Deu, E., Verdoes, M., and Bogyo, M. (2012) New approaches for dissecting protease functions to improve probe development and drug discovery. *Nat Struct Mol Biol*. 19, 9–16**
4. **Zhang, Q., Wu, D., Lin, Y., Wang, X., Kong, H., and Tanaka, S. (2015) Substrate and Product Inhibition on Yeast Performance in Ethanol Fermentation. *Energy Fuels*. 29, 1019–1027**
5. **Fan, R., Ebrahimi, M., and Czermak, P. (2017) Anaerobic Membrane Bioreactor for Continuous Lactic Acid Fermentation. *Membranes*. 7, 26**
6. **Middleton, R. J. (1990) Hexokinases and glucokinases. *Biochem. Soc. Trans*. 18, 180–183**
7. **Uchiyama, T., Miyazaki, K., and Yaoi, K. (2013) Characterization of a Novel β-Glucosidase from a Compost Microbial Metagenome with Strong Transglycosylation Activity *. *J. Biol. Chem*. 288, 18325–18334**
8. **Matsuzawa, T., and Yaoi, K. (2017) Screening, identification, and characterization of a novel saccharide-stimulated β-glycosidase from a soil metagenomic library. *Appl Microbiol Biotechnol*. 101, 633–646**
9. **Wang, F., Chen, L., Arcucci, O., Harvey, E. V., Bowers, B., Xu, Y., Hammer, J. A., and**

Sellers, J. R. (2000) Effect of ADP and Ionic Strength on the Kinetic and Motile Properties of Recombinant Mouse Myosin V *. *J. Biol. Chem.* 275, 4329–4335

10. De La Cruz, E. M., Sweeney, H. L., and Ostap, E. M. (2000) ADP Inhibition of Myosin V ATPase Activity. *Biophys. J*. 79, 1524–1529

11. Drew, J. S., Harwalkar, V. A., and Stein, L. A. (1992) Product inhibition of the actomyosin subfragment-1 ATPase in skeletal, cardiac, and smooth muscle. *Circ. Res*. 71, 1067–1077

12. Yamashita, H., Sata, M., Sugiura, S., Momomura, S., Serizawa, T., and Iizuka, M. (1994) ADP inhibits the sliding velocity of fluorescent actin filaments on cardiac and skeletal myosins. *Circ. Res*. 74, 1027–1033

13. Vasilyeva, E. A., Minkov, I. B., Fitin, A. F., and Vinogradov, A. D. (1982) Kinetic mechanism of mitochondrial adenosine triphosphatase. ADP-specific inhibition as revealed by the steady-state kinetics. *Biochem. J*. 202, 9–14

14. Milgrom, Y. M., and Boyer, P. D. (1990) The ADP that binds tightly to nucleotide-depleted mitochondrial F1-ATPase and inhibits catalysis is bound at a catalytic site. *Biochim. Biophys. Acta*. 1020, 43–48

15. Jault, J. M., and Allison, W. S. (1993) Slow binding of ATP to noncatalytic nucleotide binding sites which accelerates catalysis is responsible for apparent negative cooperativity exhibited by the bovine mitochondrial F1-ATPase. *J. Biol. Chem*. 268, 1558–1566

16. Jault, J.-M., Dou, C., Grodsky, N. B., Matsui, T., Yoshida, M., and Allison, W. S. (1996) The α3β3γ Subcomplex of the F1-ATPase from the Thermophilic *Bacillus* PS3 with the βT165S Substitution Does Not Entrap Inhibitory MgADP in a Catalytic Site during Turnover*. *J. Biol. Chem*. 271, 28818–28824

17. Muneyuki, E., Watanabe-Nakayama, T., Suzuki, T., Yoshida, M., Nishizaka, T., and Noji, H. (2007) Single Molecule Energetics of F1-ATPase Motor. *Biophys. J*. 92, 1806–1812

18. Gibbons, I. R., Gibbons, B. H., Mocz, G., and Asai, D. J. (1991) Multiple nucleotide-binding sites in the sequence of dynein β heavy chain. *Nature*. 352, 640–643

19. Ogawa, K. (1991) Four ATP-binding sites in the midregion of the β heavy chain of dynein. *Nature*. 352, 643–645

20. Yagi, T. (2000) ADP-dependent Microtubule Translocation by Flagellar Inner-Arm Dyneins. *Cell Struct. Funct.* 25, 263–267

21. Shiroguchi, K., and Toyoshima, Y. Y. (2001) Regulation of monomeric dynein activity by ATP and ADP concentrations. *Cell Motil. Cytoskeleton*. 49, 189–199

22. Ishibashi, K., Sakakibara, H., and Oiwa, K. (2020) Force-Generating Mechanism of Axonemal Dynein in Solo and Ensemble. *Int. J. Mol. Sci.* 21, 2843

23. Schief, W. R., Clark, R. H., Crevenna, A. H., and Howard, J. (2004) Inhibition of kinesin

motility by ADP and phosphate supports a hand-over-hand mechanism. *Proc. Natl. Acad. Sci. U.S.A.* 101, 1183–1188

24. Hirokawa, N., Noda, Y., Tanaka, Y., and Niwa, S. (2009) Kinesin superfamily motor proteins and intracellular transport. *Nat Rev Mol Cell Biol*. 10, 682–696

25. Peden, E. M., and Barr, M. M. (2005) The KLP-6 Kinesin Is Required for Male Mating Behaviors and Polycystin Localization in Caenorhabditis elegans. *Curr. Biol*. 15, 394–404

26. Morsci, N. S., and Barr, M. M. (2011) Kinesin-3 KLP-6 Regulates Intraflagellar Transport in Male-Specific Cilia of Caenorhabditis elegans. *Curr. Biol*. 21, 1239–1244

27. Okada, Y., and Hirokawa, N. (1999) A Processive Single-Headed Motor: Kinesin Superfamily Protein KIF1A. *Science*. 283, 1152–1157

28. Kita, T., Chiba, K., Wang, J., Nakagawa, A., and Niwa, S. (2024) Comparative analysis of two Caenorhabditis elegans kinesins KLP-6 and UNC-104 reveals a common and distinct activation mechanism in kinesin-3. *eLife*. 12, RP89040

29. Kita, T., Sasaki, K., and Niwa, S. (2025) Biased movement of monomeric kinesin-3 KLP-6 explained by a symmetric Brownian ratchet model. *Biophys. J*. 124, 205–214

30. Soppina, V., Norris, S. R., Dizaji, A. S., Kortus, M., Veatch, S., Peckham, M., and Verhey, K. J. (2014) Dimerization of mammalian kinesin-3 motors results in superprocessive motion. *Proc. Natl. Acad. Sci. U.S.A*. 111, 5562–5567

31. Budaitis, B. G., Jariwala, S., Rao, L., Yue, Y., Sept, D., Verhey, K. J., and Gennerich, A. (2021) Pathogenic mutations in the kinesin-3 motor KIF1A diminish force generation and movement through allosteric mechanisms. *J. Cell Biol.* 220, e202004227

32. Boyle, L., Rao, L., Kaur, S., Fan, X., Mebane, C., Hamm, L., Thornton, A., Ahrendsen, J. T., Anderson, M. P., Christodoulou, J., Gennerich, A., Shen, Y., and Chung, W. K. (2021) Genotype and defects in microtubule-based motility correlate with clinical severity in KIF1A-associated neurological disorder. *HGG Adv*. 2, 100026

33. Anazawa, Y., Kita, T., Iguchi, R., Hayashi, K., and Niwa, S. (2022) De novo mutations in KIF1A-associated neuronal disorder (KAND) dominant-negatively inhibit motor activity and axonal transport of synaptic vesicle precursors. *Proc. Natl. Acad. Sci. U.S.A.* 119, e2113795119

34. Kita, T., Sasaki, K., and Niwa, S. (2023) Modeling the motion of disease-associated KIF1A heterodimers. *Biophys. J*. 122, 4348–4359

35. Lu, H., Ali, M. Y., Bookwalter, C. S., Warshaw, D. M., and Trybus, K. M. (2009) Diffusive Movement of Processive Kinesin-1 on Microtubules. *Traffic*. 10, 1429–1438

36. Lam, A. J., Rao, L., Anazawa, Y., Okada, K., Chiba, K., Dacy, M., Niwa, S., Gennerich, A., Nowakowski, D. W., and McKenney, R. J. (2021) A highly conserved 310 helix within the kinesin motor domain is critical for kinesin function and human health. *Sci. Adv*. 7,

eabf1002

37. Hancock, W. O., and Howard, J. (1999) Kinesin's processivity results from mechanical and chemical coordination between the ATP hydrolysis cycles of the two motor domains. *Proc. Natl. Acad. Sci. U.S.A.* 96, 13147–13152

38. Motojima, F., and Yoshida, M. (2003) Discrimination of ATP, ADP, and AMPPNP by Chaperonin GroEL: HEXOKINASE TREATMENT REVEALED THE EXCLUSIVE ROLE OF ATP*. *J. Bio. Chem*. 278, 26648–26654

39. You, H., Lattmann, S., Rhodes, D., and Yan, J. (2017) RHAU helicase stabilizes G4 in its nucleotide-free state and destabilizes G4 upon ATP hydrolysis. *Nucleic Acids Res*. 45, 206–214

40. Zaniewski, T. M., and Hancock, W. O. (2023) Positive charge in the K-loop of the kinesin-3 motor KIF1A regulates superprocessivity by enhancing microtubule affinity in the one-head–bound state. *J. Biol. Chem*. 299, 102818

41. Pan, X., Ou, G., Civelekoglu-Scholey, G., Blacque, O. E., Endres, N. F., Tao, L., Mogilner, A., Leroux, M. R., Vale, R. D., and Scholey, J. M. (2006) Mechanism of transport of IFT particles in C. elegans cilia by the concerted action of kinesin-II and OSM-3 motors. *J Cell Biol*. 174, 1035–1045

42. Kikkawa, M., Sablin, E. P., Okada, Y., Yajima, H., Fletterick, R. J., and Hirokawa, N. (2001) Switch-based mechanism of kinesin motors. *Nature*. 411, 439–445

43. Wang, W., Ren, J., Song, W., Zhang, Y., and Feng, W. (2022) The architecture of kinesin-3 KLP-6 reveals a multilevel-lockdown mechanism for autoinhibition. *Nat Commun*. 13, 4281

44. Vale, R. D. (2003) The Molecular Motor Toolbox for Intracellular Transport. *Cell*. 112, 467–480

45. Nitta, R., Kikkawa, M., Okada, Y., and Hirokawa, N. (2004) KIF1A Alternately Uses Two Loops to Bind Microtubules. *Science*. 305, 678–683

46. Behnke-Parks, W. M., Vendome, J., Honig, B., Maliga, Z., Moores, C., and Rosenfeld, S. S. (2011) Loop L5 Acts as a Conformational Latch in the Mitotic Kinesin Eg5*. *J. Biol. Chem*. 286, 5242–5253

47. Traut, T. W. (1994) Physiological concentrations of purines and pyrimidines. *Mol Cell Biochem*. 140, 1–22

48. Akter, M., Keya, J. J., Kayano, K., Kabir, A. M. R., Inoue, D., Hess, H., Sada, K., Kuzuya, A., Asanuma, H., and Kakugo, A. (2022) Cooperative cargo transportation by a swarm of molecular machines. *Sci. Robot*. 7, eabm0677

49. Kawamata, I., Nishiyama, K., Matsumoto, D., Ichiseki, S., Keya, J. J., Okuyama, K., Ichikawa, M., Kabir, A. Md. R., Sato, Y., Inoue, D., Murata, S., Sada, K., Kakugo, A., and

Nomura, S. M. (2024) Autonomous assembly and disassembly of gliding molecular robots regulated by a DNA-based molecular controller. *Sci. Adv.* 10, eadn4490

50. Castoldi, M., and Popov, A. V. (2003) Purification of brain tubulin through two cycles of polymerization–depolymerization in a high-molarity buffer. *Protein Expr. Purif.* 32, 83–88

51. Kita, T., and Niwa, S. Total Internal Reflection Fluorescence (TIRF) Single-Molecule Assay to Analyze the Motility of Kinesin. *Bio-protocol*. 14, e5135

52. Schneider, C. A., Rasband, W. S., and Eliceiri, K. W. (2012) NIH Image to ImageJ: 25 years of image analysis. *Nat Methods*. 9, 671–675

53. Robert, X., and Gouet, P. (2014) Deciphering key features in protein structures with the new ENDscript server. *Nucleic Acids Res*. 42, W320–W324

54. Šali, A., and Blundell, T. L. (1993) Comparative Protein Modelling by Satisfaction of Spatial Restraints. *J. Mol. Biol.* 234, 779–815

55. Khatib, F., Cooper, S., Tyka, M. D., Xu, K., Makedon, I., Popović, Z., Baker, D., and Players, F. (2011) Algorithm discovery by protein folding game players. *Proc. Natl. Acad. Sci. U.S.A.* 108, 18949–18953

56. Maguire, J. B., Haddox, H. K., Strickland, D., Halabiya, S. F., Coventry, B., Griffin, J. R., Pulavarti, S. V. S. R. K., Cummins, M., Thieker, D. F., Klavins, E., Szyperski, T., DiMaio, F., Baker, D., and Kuhlman, B. (2021) Perturbing the energy landscape for improved packing during computational protein design. *Proteins:Struct., Funct., Bioinf.* 89, 436–449

Figure legends

Figure 1 Directional movements of KLP-6(1-390)LZ in an ADP solution

(A) Schematic illustration of the domain organization in KIF1A(1-393)LZ and KLP-6(1-390)LZ tagged with a fluorescent protein mScarlet-I.

(B) Representative kymographs showing the motility of KIF1A(1-393)LZ and KLP-6(1-390)LZ in the presence of 2 mM Mg·ADP purchased from Nacarai tesque. Scale bars: horizontal, 5 µm; vertical, 10 seconds.

(C) Histogram of velocity for KLP-6(1-390)LZ in the presence of 2 mM Mg·ADP. n = 129

(D) Representative kymograph showing the motility of KLP-6(1-390)LZ in the presence of 2 mM Mg·HK-ADP. Scale bars: horizontal, 5 µm; vertical, 10 seconds.

Figure 2 Minimum ADP inhibition in KLP-6(1-390)LZ

(A) Representative kymographs showing the motility of KIF1A(1-393)LZ in the presence of 1 mM Mg·ATP, with or without an additional 1 mM Mg·HK-ADP. Scale bars: horizontal, 5 µm; vertical, 10

seconds.

(B) Single-molecule velocity of KIF1A(1-393)LZ versus [Mg·ATP] in the absence (circles) and presence (diamonds) of 1 mM HK-ADP. The black and orange solid lines represent the regression curves fitted to the Michaelis-Menten equation and the equation with product inhibition, respectively. Each data point represents the mean ± S.E. At least three independent experiments were conducted for each condition, with more than 114 motile particles analyzed."

(C) Representative kymographs showing the motility of KLP-6(1-390)LZ in the presence of 1 mM Mg·ATP, with or without an additional 1 mM Mg·HK-ADP, and in the presence of 100 μM Mg·ATP, with or without an additional 1 mM Mg·HK-ADP. Scale bars: horizontal, 5 μm; vertical, 10 seconds.

(D) Single-molecule velocity of KLP-6(1-390)LZ versus [Mg·ATP] in the absence (circles) and presence (diamonds) of 1 mM HK-ADP. The black and orange solid lines represent the regression curves fitted to the Michaelis-Menten equation and the equation with product inhibition, respectively. Each data point represents the mean ± S.E. At least three independent experiments were conducted for each condition, with more than 131 motile particles analyzed."

(E-H) Comparison of (E) $V_{\max}$, (F) K_{M} (G) K_{I} and (H) $K_{\mathrm{I}}/K_{\mathrm{M}}$ between KIF1A(1-393)LZ and KLP-6(1-390)LZ. Error bars represent the mean ± S.E.

Figure 3 Amino acid sequence and structural comparison between KLP-6 and other kinesin-3s

(A) Alignment of kinesin-3 amino acid sequences. Identical residues are highlighted in black, while highly conserved residues are outlined with a black border. The secondary structures of KLP-6 are indicated at the bottom. KLP-6-specific residues are highlighted in magenta.

(B) Protein structure of the motor domain of *Mus musculus* KIF1A bound to Mg·ADP (PDB: 1I5S). Loop-3 and highly conserved residues (T106, M107, and M108) are highlighted in magenta. K110, also highlighted in magenta, forms a hydrogen bond with the ADP-ribose.

(C) Protein structure of the motor domain of *C. elegans* KLP-6 bound to Mg·ADP (PDB: 7WRG). This structure was derived from the full-length KLP-6 structure, with all domains other than the motor domain (with Mg·ADP) removed for visualization. Loop-3 and KLP-6-specific residues (S116, I117, and V118) are highlighted in magenta. F120, corresponding to K110 in KIF1A, is also highlighted in magenta.

Figure 4 Role of domains in the minimal ADP inhibition of KLP-6(1-390)LZ

(A) Mutation sites in KLP-6(1-390)LZ. In KLP-6(1-390)LZ(L3SW), amino acids 60–73 are replaced with amino acids 60–63 from KIF1A.

(B) SDS-PAGE analysis of KLP-6(1-390)LZ and its mutants. M represents the marker lane. Numbers on the left indicate molecular weight (kDa).

(C) Representative kymographs showing the motility of KLP-6(1-390)LZ(L3SW),

KLP-6(1-390)LZ(F120K), and KLP-6(1-390)LZ(SIV/TMM) in the presence of 1 mM Mg·ATP, with or without an additional 1 mM Mg·HK-ADP, and in the presence of 100 μM Mg·ATP, with or without an additional 1 mM Mg·HK-ADP. Scale bars: horizontal, 5 μm; vertical, 10 seconds.

(D-F) Single-molecule velocity of KLP-6(1-390)LZ(L3SW), KLP-6(1-390)LZ(F120K), and KLP-6(1-390)LZ(SIV/TMM) versus [Mg·ATP] in the absence (circles) and presence (diamonds) of 1 mM HK-ADP. The black and orange solid lines represent the regression curves fitted to the Michaelis-Menten equation and the equation with product inhibition, respectively. The faint black and orange solid lines indicate the results for KLP-6(1-390)LZ, as shown in Fig. 2D. Each data point represents the mean ± S.E. At least three independent experiments were conducted for each condition, with more than 150 motile particles analyzed."

(G-J) Comparison of (E) $V_{\max}$, (F) K_{M} (G) K_{I} and (H) $K_{\mathrm{I}}/K_{\mathrm{M}}$ between KLP-6(1-390)LZ, KLP-6(1-390)LZ(L3SW), KLP-6(1-390)LZ(F120K), and KLP-6(1-390)LZ(SIV/TMM). Error bars represent the mean ± S.E.

Table 1. Summary of the kinetic parameters

	CeKinesin-3				**HsKinesin-3**	**DmKinesin-1***	**CeKinesin-2#**
	KLP-6	KLP-6 (L3SW)	KLP-6 (F120K)	KLP-6 (SIV/TMM)	KIF1A	KIF5B	KLP-11/KLP-20/KAP-1
$V_{\max}$ (nm/s)	248±3	203±5	338±4	234±3	2381±23	906±9	260
K_{M} (μM)	20.1±0.5	31.3±1.7	20.3±0.5	4.4±0.1	190±3	28.1±0.9	280
K_{I} (μM)	901±31	1175±78	242±4	11.9±0.3	247±3	34.6±2.6	42
$K_{\mathrm{I}}/K_{\mathrm{M}}$	44.9±1.9	37.5±2.9	11.9±0.6	2.7±0.3	1.3±0.1	1.2±0.1	0.15

Values are mean±S.E.

*, data from Schief et al.(2004) (23)

#, data from Pan et al. (2006) (41)

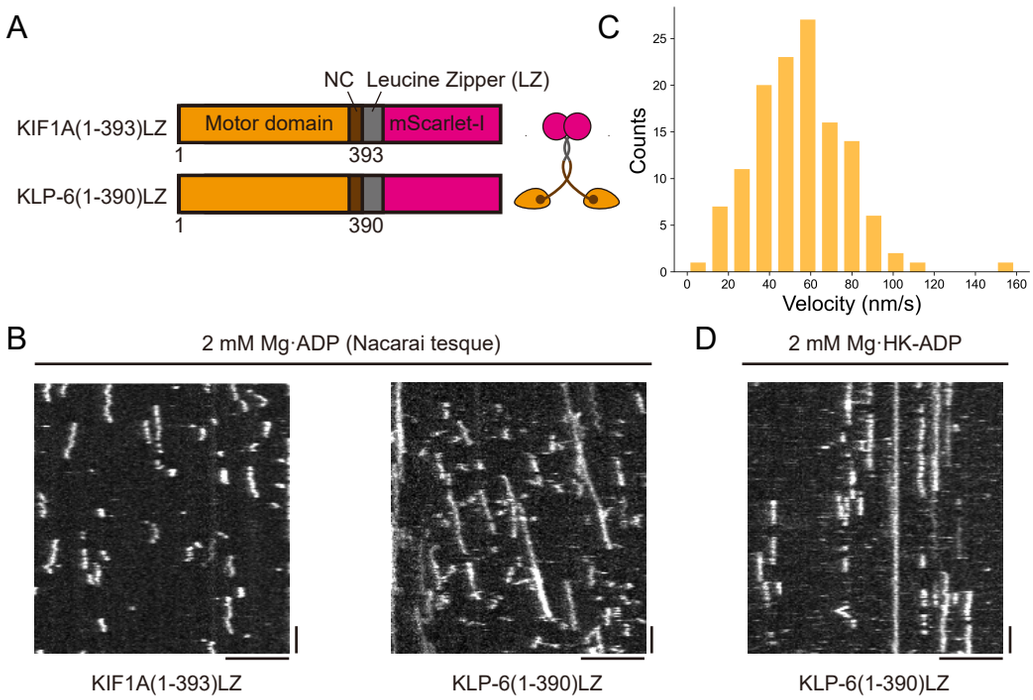

Kita and Niwa Figure 1

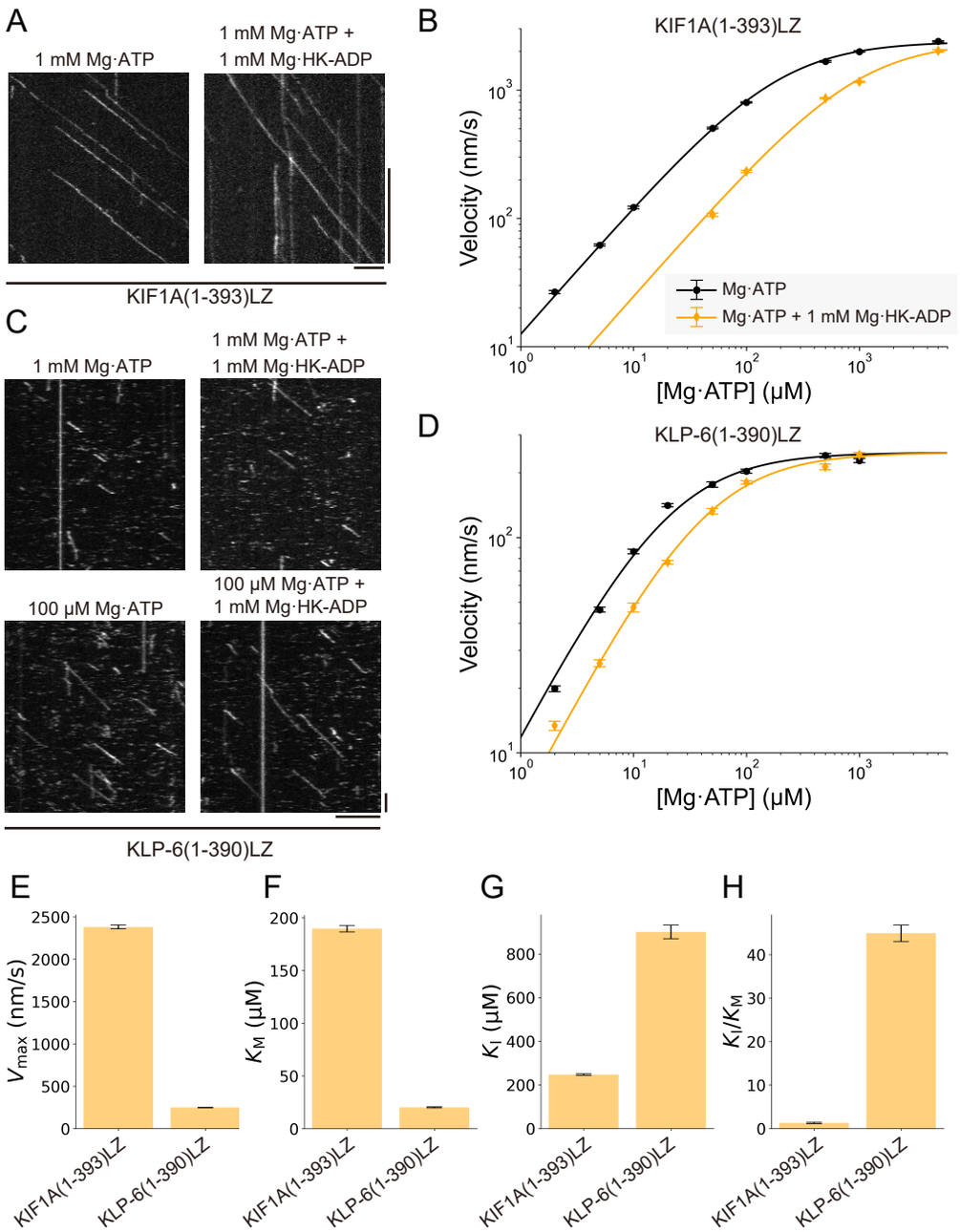

Kita and Niwa Figure 2

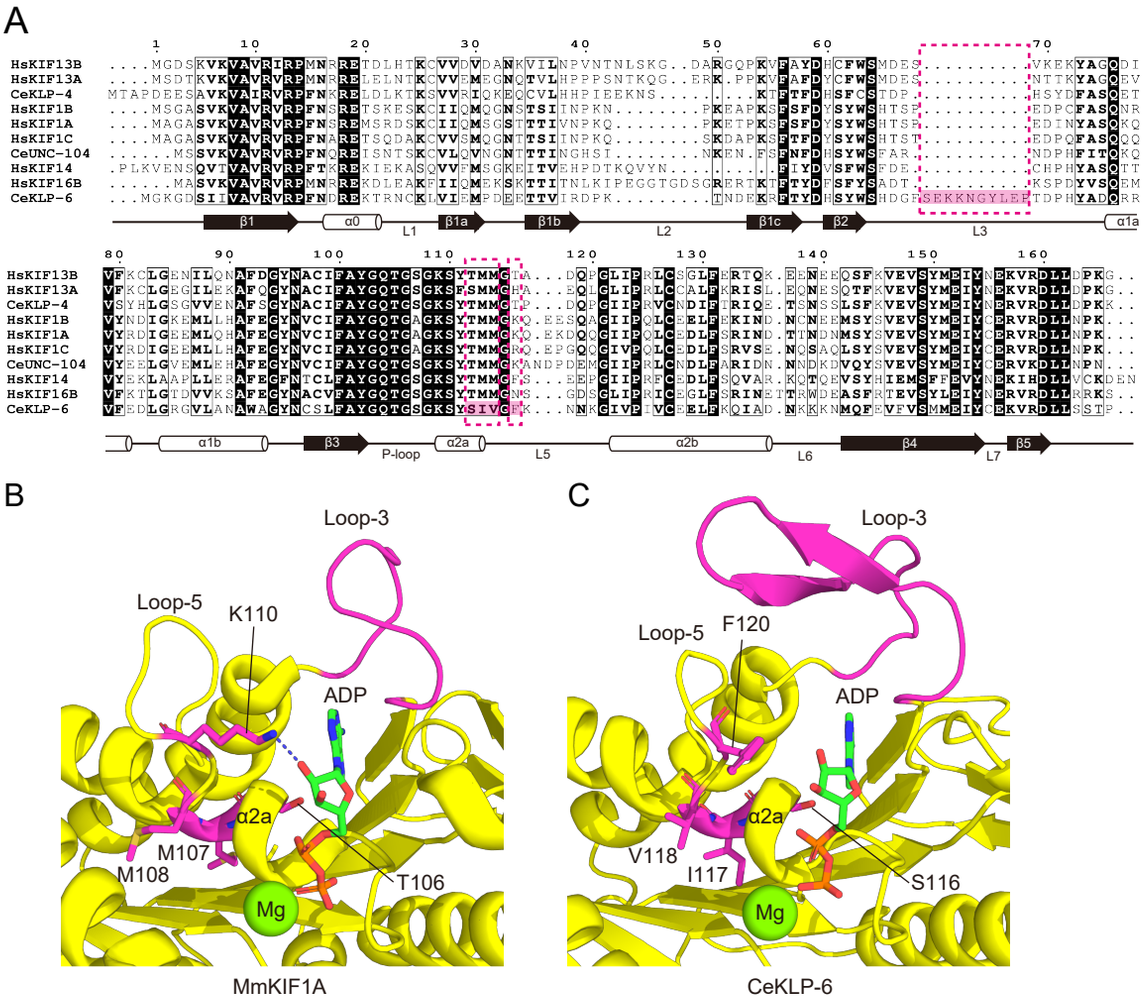

Kita and Niwa Figure 3

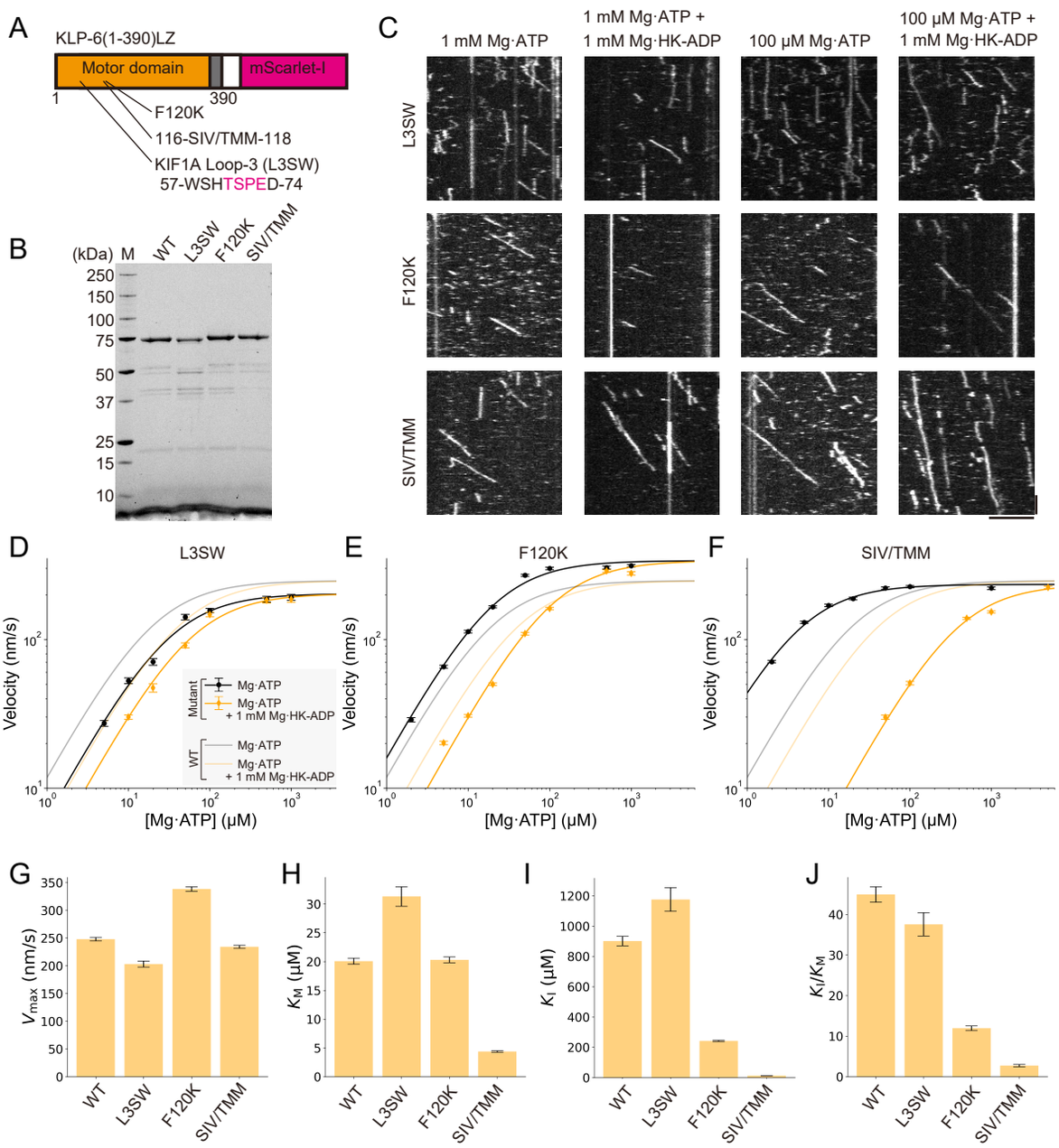

Kita and Niwa Figure 4